# FORMULATION OF A COMPUTATIONAL AEROELASTIC MODEL TO PREDICT TRIM AND RESPONSE OF A HELICOPTER ROTOR SYSTEM

V. Laxman* and C. Venkatesan**

**Abstract**

*Comparison of theoretical and experimental data (flight test data) reveals that still there is a gap between theory and experiment. Some of the observed phenomenon in flight test may be due to the nonlinearities associated with the aeroelastic problems and this paper attempts to develop a theoretical formulation including the geometrical nonlinearities associated with structural modeling and the aerodynamic nonlinearities associated with dynamic stall. In this paper, the consolidated set of equations representing blade dynamics, rotor inflow and sectional aerodynamics are presented. The iterative computational solution technique developed for trim and response analysis is described and a systematic study is undertaken to analyse the influence of various aerodynamic models, representing rotor inflow and sectional loads, on the helicopter trim and aeroelastic response of the rotor blades. It is also shown that the structural coupling due to blade pretwist significantly influences the rotor blade response and loads compared to an untwisted rotor blade.*

**Nomenclature**

$a_d$, $a_1$, $a_m$ = parameters used in dynamic stall model
b = blade semi-chord
$C_D$ = unsteady drag coefficient
$C_{dL}$ = linear static drag coefficient extrapolated to the stall region
$C_M$ = unsteady moment coefficient
$C_{mL}$ = linear static moment coefficient extrapolated to the stall region
$C_t$ = chord of the tail rotor
$C_T$ = main rotor thrust coefficient
$C_{Tt}$ = tail rotor thrust coefficient
$C_Z$ = unsteady lift coefficient
$C_{zL}$ = linear static lift coefficient extrapolated to the stall region
$C_{D0}$ = zero-lift drag coefficient
$[\overline{C}]$ = damping matrix in modal space
d, $d_m$ = parameters used in dynamic stall model
D = drag on airfoil or fuselage drag
f = fuselage frontal area
$\{\overline{F}\}$ = generalized aerodynamic load vector
H = longitudinal force
$k_x$, $k_y$ = inflow parameters in Drees model
$K_n^m$ = parameter used in dynamic wake model, $\frac{2}{\pi} H_n^m$
$[\overline{K}]$ = stiffness matrix in modal space
L = lift on airfoil
[L] = coupling or gain matrix
$[\tilde{L}^c]$, $[\tilde{L}^s]$ = cosine and sine influence coefficient matrices
M = moment on airfoil about elastic axis or Mach number
$M_x$,$M_y$,$M_z$ = rolling, pitching and yawing moment
[M] = mass matrix or apparent mass matrix in inflow model
$[\overline{M}]$ = mass matrix in modal space
n, j = polynomial number
$N_b$ = number of blades
$P_j^p(\bar{\upsilon})$ = Legendre polynomial functions
$\overline{P}_j^p(\bar{\upsilon})$ = normalised Legendre polynomial functions, $(-1)^p P_j^p(\bar{\upsilon})/\rho_j^p$
r = radial distance
r = nondimensional radial coordinate, $\frac{r}{R}$
$r_d$, $r_l$, $r_m$ = parameters used in dynamic stall model

* Graduate Student ** Pandit Ramachandra Dwivedi Chair Professor
Department of Aerospace Engineering, Indian Institute of Technology Kanpur, Kanpur-208 018, India, Email : cven@iitk.ac.in
Manuscript received on 06 Aug 2008; Paper reviewed, revised and accepted on 27 May 2009

$R$ = rotor blade radius
$R_t$ = radius of the tail rotor
$\tilde{S}$ = area of airfoil
$s_h$ = horizontal tail area
$s_v$ = vertical tail area
$t$ = time
$T$ = main rotor thrust force
$T_t$ = tail rotor thrust force
$V$ = oncoming velocity
$V_F$ = velocity at helicopter centre of mass
$V_H$ = velocity of the hub
$V_T$, $V_R$ = velocity terms used in inflow models
$[V]$, $[V_c]$, $[V_s]$ = velocity matrices used in dynamic inflow models
$W$ = weight of the helicopter
$X$, $l$ = parameters defined in dynamic wake model
$Y$ = lateral force
$\alpha$ = rotor shaft tilt angle w.r.t. helicopter forward velocity
$\tilde{\alpha}$, $\tilde{k}$ = parameters used in dynamic stall model
$\alpha_j^p$, $\beta_j^p$ = induced flow coefficients
$\chi$ = wake skew angle
$\Delta t$ = time step
$\phi_j^p$ = radial shape functions
$\Phi$ = fuselage attitude in roll
$\Gamma_1$ = aerodynamic state in unstalled region in lift equation
$\Gamma_2$ = aerodynamic state in stalled region in lift equation
$\Gamma_{d2}$ = aerodynamic state in stalled region in drag equation
$\Gamma_{m2}$ = aerodynamic state in stalled region in moment equation
$\lambda$ = total inflow ratio
$\lambda_i$ = induced inflow ratio
$\lambda_u$, $\lambda_0$ = uniform inflow ratio
$\lambda_t$ = tail rotor inflow
$\{\eta\}$ = vector of modal degrees of freedom
$\mu$ = advance ratio
$\theta$ = pitch angle in degree
$\theta_{FP}$ = flight path angle
$\theta_0$ = main rotor collective pitch angle
$\theta_{0T}$ = tail rotor collective pitch angle
$\theta_{1c}$, $\theta_{ls}$ = cyclic pitch angles
$\Theta$ = fuselage attitude pitch
$\rho$ = density of air
$\rho_j^p$ = normalised factor used in dynamic wake model, $\sqrt{\frac{(j+p)!!}{(2j+1)!!\,(j-p)!!}}$
$\sigma$, $\sigma_d$, $\sigma_m$ $\overline{\sigma}_m$ = parameters used in dynamic stall model
$\sigma_t$ = tail rotor solidity ratio
$\tau_n^{mc}$, $\tau_n^{ms}$ = coefficients of pressure expansion
$\Omega$ = rotational speed (frequency) of the rotor
$\Omega_t$ = tail rotor rotating speed
$\psi$ = azimuthal angle or nondimentional time, $\Omega t$
$\psi_k$ = azimuthal angle of the $k^{th}$ blade
$(\,)_{lk}$ = quantities in rotating *1k* coordinate system
$(\,)_{3k}$ = quantities in rotating *3k* coordinate system
$(\dot{\,})$ = derivative w.r.t. time

## Introduction

Formulation and analysis of rotary-wing aeroelastic/aeromechanical problems require an understanding of wide range of disciplines like, continuum mechanics, unsteady aerodynamics including stall effects, and control techniques. It is well known that helicopter rotor blades are long slender beams undergoing moderate structural deformations involving coupled flap (out-of-plane bending), lag (in-plane bending), torsion and axial modes. Therefore, a thorough knowledge of continuum mechanics is necessary for the development of structural models for rotor blades. Unlike aircraft wings, the helicopter rotor blades operate in a highly complex aerodynamic environment where different cross-sections of the blade undergo different adverse aerodynamic phenomena, like, dynamic stall, reverse flow, compressibility effects, radial flow and blade-vortex interaction.

Aeroelastic stability and response of rotor blade under hovering and forward flight conditions have been studied extensively by several researchers. An excellent review on the developments of rotary-wing aeroelasticity is presented in Refs. [1] -[6]. From the references ([4] -[6]), it is clear that the structural dynamic modeling of the rotor blade representing all the geometric complexities of the rotor system and the coupled flap-lag-axial-torsion motions of the blade has reached a high level of sophistication. While formulating the aerodynamic operator, one should consider (a) unsteady aerodynamics of a rotor

blade undergoing coupled pitching-plunging motion in a time varying oncoming flow, (b) induced flow (or inflow) at the rotor disc due to rotor blade wake, and (c) dynamic stall. Earlier studies used inflow models derived from momentum theory and quasi-steady aerodynamic models for the evaluation of sectional loads. With the development of perturbation inflow and dynamic inflow models, several studies employed these models in their analysis (Refs. [7] -[10]).

The application of dynamic wake model for rotor analysis was attempted for the first time by Ay Su and Peters (Refs. [11] and [12]). The results showed that there is a significant effect of unsteady aerodynamics on the damping of all the flap modes of the rotor. Manjunath [13], applied dynamic wake model for his work on rotor stability in hover and forward flight. The results (Refs. [13] and [14]) indicated that analysis with dynamic wake model showed an improved correlation with the test data. The results also showed that for a better prediction of damping at least three radial functions with each harmonic of the wake states are required in dynamic wake model. The dynamic wake model was applied to investigate the aeromechanical stability of a rotor-fuselage system under hover and forward flight conditions (Ref. [15]). The theoretical model was validated by comparing the analytical results with experimental data on ground resonance of a model helicopter. In all these studies, dynamic stall effects were not considered.

Tran and Falchero [16] have applied the ONERA stall model to study the stability and response of an isolated rotor blade in hover and forward flight. A nonuniform inflow model has been used for the induced inflow calculation. Rogers [17] has applied the simplified version of ONERA stall model to analyse stabilty and response of a single section model of a helicopter blade under-going flapping motion. Several other researchers (Refs. [18] - [20]) have also applied the dynamic stall model in the aeroelastic stability and response studies of rotor blades. The effect of dynamic stall on flap-lag stability of rotor blade is analysed by Barwey et al. (Refs. [21] and [22]) and Tang et al. ([23]). The results of all these studies showed that the dynamic stall effects improve the correlation with experimental data as compared to quasi-steady aerodynamic model.

In recent years, several aeroelastic studies were undertaken by combining different aerodynamic models representing the rotor wake effects (dynamic wake models) and the unsteady aerodynamic loads (ONERA dynamic stall models) on a typical section of a rotor blade. Peters et al. [24] have developed a suitable formulation by combining ONERA stall model and dynamic wake model for rotor blade aeroelastic and control analysis. Chunduru et al. [25] investigated the effects of dynamic stall and 3-D wake on trim and lag damping of isolated bearingless rotors. They concluded that dynamic stall and wake effects appreciably improve the correlation between theory and experiment for lag damping which is given as a function of forward speed. In a subsequent study, Subramanian et al. [26] investigated a hierarchy of aerodynamic models. Their work mainly focused on the prediction of trim settings, regressive lag-mode damping, and root flap moment.

Prediction of rotor loads and blade response, using a combination of computational fluid dynamics (CFD) and computational structural dynamics (CSD) has been studied by various research groups (Refs. [27] - [29]). In Refs. [27] and [28], the studies essentially focused on predicting the blade loads for steady and level flight. Whereas, Bhagwat et al. (Ref. [29]) have focused on predicting the blade loads for the case of maneuvering flight. All these studies focused on correlating the theoretical results with the flight test data of UH-60A.

In Refs. [30-31], it is reported that vibration in the helicopter is significantly influenced by frequencies other than blade passage frequency and its integer multiples ($bN_b$/rev, b = 1,2,3,..., where $N_b$ is the number of blades in the rotor system). In a recent study reported in Ref. [32], the authors have observed that the vibratory signals obtained at different locations in the fuselage contain a wide spectrum of frequency contents including those below Nb/rev. There is no published open literature available on theoretical studies addressing the issue of frequencies below Nb/rev on the rotor vibratory loads. Some of the observed phenomenon in flight test may be attributed to the nonlinearities associated with the aeroelastic problem.

Accurate prediction of rotor loads in all the flight conditions using CFD/CSD coupling (computational aeroelasticity) analysis is however still beyond the current state of the art. While development of this field can have major benefits in the prediction of rotor loads and response in the long run, the need for simpler, yet efficient and less time-consuming models for real-time simulations persists. The motivation for the present study is develop a computational aeroelastic analysis for the prediction of trim and rotor loads for a realistic helicopter configuration. The development of the code has been made in modular form

so that any advances in structural and/or aerodynamic modeling can be incorporated easily.

The theoretical formulation includes geometrical nonlinearities associated with structural modeling and aerodynamic nonlinearities associated with dynamic stall. However for purpose of comparison, several combinations of aerodynamic models (inflow modeling and sectional aerodynamic modeling) have been analysed. The inflow models can be categorized as: (i) uniform inflow model based on momentum theory, (ii) Drees model, and (iii) dynamic wake model. The sectional aerodynamic loads can be evaluated by either (i) quasi-steady approximation of Greenberg's theory applicable for only attached flow conditions or by (ii) dynamic stall model applicable for both attached and separated flow. In the present study, five different combinations of aerodynamic models have been proposed and the influence of each one of these models on the trim and response characteristics of helicopter rotor in forward flight is analysed systematically.

The objectives of the present study are:

- Development of a structural dynamic model for a flexible rotor blade with and without pretwist.
- Formulation of a time domain computational aeroelastic model by integrating the structural model, the inflow model, and the dynamic stall model for the prediction of trim and response of a helicopter rotor system in forward flight.
- Formulation of a suitable computational technique for the evaluation of trim and response of a multi-bladed helicopter rotor system in forward flight. Perform a systematic analysis to identify the effects of aerodynamic modeling on the trim settings.
- Study the effects of forward speeds on rotor loads and blade response of a realistic helicopter.
- Study the effects of structural couplings due to blade pretwist on blade response and rotor loads of a realistic helicopter.

## Formulation

Helicopter trim and response calculation requires all the loads acting on the helicopter system. The loads are due to (i) main rotor system (acting at the rotor hub), (ii) fuselage aerodynamic load, (iii) tail rotor hub loads, (iv) horizontal tail and vertical tail loads and (v) gravity effects. For the sake of clarity, a brief description of the loads acting on various aerodynamic surfaces is given below.

### Main Rotor

Evaluation of aerodynamic loads requires the motion of the blade at every instant. A nonlinear strain-displacement model is used to describe the coupling between axial, bending and torsional deformations. The coupled equations of motion have been derived using Hamilton's principle. In the formulation of the equations of motion of a rotor blade under going moderate deformations, a large number of higher order terms are generated. In order to identify and eliminate higher order terms in a consistent manner, an ordering scheme is employed. The rotor blade is modeled using beam-type finite elements, and each element has 14 degrees of freedom. This model is identical to the model developed in Ref. [33]. A linear structural dynamic problem is first solved in finite element domain to obtain the rotating mode shapes and frequencies of the rotor blade. The blade response is evaluated in modal space in rotating system with four flap modes, two lag modes, one torsion, and one axial mode. The equations of motion in modal space can be written as:

$$[\bar{M}]\{\ddot{\eta}\} + [\bar{C}]\{\dot{\eta}\} + [\bar{K}]\{\eta\} = \{\bar{F}\} \tag{1}$$

where $\{\bar{F}\}$ represents the generalized aerodynamic load and all the nonlinear terms associated with inertia operator of the blade.

### Inflow Model

The aerodynamic model requires evaluation of rotor inflow as a function of azimuth and radial distance. In this paper, three types of global inflow models, namely, steady uniform inflow model, Drees model and dynamic wake model, are considered. A brief mathematical description of these models is provided in the following.

i). Uniform Inflow Model

In uniform inflow model, the total inflow through the rotor disc is assumed a constant and is given as:

$$\lambda_u = \mu \tan \alpha + \lambda_i \tag{2}$$

where

$$\lambda_i = \frac{C_T}{2\sqrt{(\mu^2 + \lambda_u^2)}}$$

ii) Drees Model

In Drees model, the rotor inflow is a function of both azimuth and radial station. It is given as :

$$\lambda(\bar{r}, \psi) = \mu \tan\alpha + \lambda_i (1 + k_x \bar{r} \sin\psi + k_y \bar{r} \cos\psi) \quad (3)$$

where

$$k_x = -2\mu \; ; \; k_y = \frac{4}{3}\left[\left(1 - 1.8\mu^2\right) \csc\chi - \cot\chi\right]$$

where $\chi$ wake skew angle and it is defined as $\chi = \tan^{-1}(\mu/\lambda_u)$.

iii) Dynamic Wake Model (Peters-He Model, Ref. [34])

In dynamic wake model, the total inflow is a function of azimuth, time and radial station. It is given as :

$$\lambda(\bar{r}, t, \psi) = \mu \tan\alpha + \sum_{p=0}^{\infty} \sum_{j=p+1, p+3}^{\infty} \phi_j^p(\bar{r}) \left[\alpha_j^p(t) \cos(p\psi) + \beta_j^p(t) \sin(p\psi)\right] \quad (4)$$

where $a_j^p$, and $\beta_j^p$ are evaluated by solving a set of differential equations.

$$[M]\left\{\dot{\alpha}_j^p\right\} + [V][\tilde{L}^c]^{-1}\left\{\alpha_j^p\right\} = \frac{1}{2}\left\{\tau_n^{mc}\right\} \quad (5)$$

and

$$[M]\left\{\dot{\beta}_j^p\right\} + [V][\tilde{L}^s]^{-1}\left\{\beta_j^p\right\} = \frac{1}{2}\left\{\tau_n^{ms}\right\} \quad (6)$$

In the above Eqs. 5 and 6, the subscripts *j*, *n* correspond to radial functions and superscripts *p, m* represent the harmonics. The linear operator [M] is associated with acceleration part of the induced flow, hence it can be called as the apparent mass matrix, and it is a diagonal matrix. $[\tilde{L}^c]$ and $[\tilde{L}^s]$ denote the cosine and sine influence coefficient matrices respectively and they depend on the wake skew angle, $\chi$. $[V_c]$ and $[V_s]$ represent velocity matrices. $\tau_n^{mc}$ and $\tau_n^{ms}$represent the cosine and sine components of the aerodynamic loads acting on the rotor system.

The cosine and sine components of the aerodynamic loads acting on the rotor system are defined in terms of blade lift weighted with radial polynomial functions $\phi_n^m(\bar{r})$. The expressions for the rotor loads are defined as:

$$\tau_n^{oc} = \frac{1}{2\pi} \sum_{k=1}^{N_b} \left[\int_0^1 \frac{L_k}{\rho \Omega^2 R^3} \phi_n^o(\bar{r}) \, d(\bar{r})\right] \quad (7)$$

$$\tau_n^{mc} = \frac{1}{\pi} \sum_{k=1}^{N_b} \left[\int_0^1 \frac{L_k}{\rho \Omega^2 R^3} \phi_n^m(\bar{r}) \, d(\bar{r})\right] \cos(m\psi_k) \quad (8)$$

$$\tau_n^{ms} = \frac{1}{\pi} \sum_{k=1}^{N_b} \left[\int_0^1 \frac{L_k}{\rho \Omega^2 R^3} \phi_n^m(\bar{r}) \, d(\bar{r})\right] \sin(m\psi_k) \quad (9)$$

where the summation is over all the blades ($N_b$) in the rotor system. $\psi_k$ represents the azimuthal location of the $k^{th}$ blade and is given by $\psi + \frac{2\pi(k-1)}{N_b}$. $L_k$ represents the lift per unit span on the $k^{th}$ blade. The sectional blade lift can be obtained from any aerodynamic theory, say for example quasi-steady Greenberg's theory, dynamic stall theory or by CFD methods.

**Sectional Aerodynamic Loads**

The sectional aerodynamic loads are evaluated by using either (i) quasi-steady approximation of Greenberg's theory or (ii) *modified* ONERA dynamic stall model applicable for both attached and separated flow. For the sake of clarity, a brief mathematical description of these models is provided.

i) Quasi-steady Greenberg's Model (Ref. [35])

The quasi-steady approximation of Greenberg's theory provides time variation of lift and moment on an oscillating airfoil. The lift, moment and drag are assumed

to be acting at the quarter chord point and the expressions are given below.

Lift acting normal to the resultant flow:

$$L = \frac{1}{2}\rho \tilde{S} b \left[ \pi \dot{W}_0 + \frac{\pi}{2} \dot{W}_1 \right] + \frac{1}{2}\rho \tilde{S} V \left[ 2\pi W_0 + 2\pi W_1 \right] \quad (10)$$

Unsteady moment about quarter chord on the airfoil is given as:

$$M = \frac{1}{2}\rho \tilde{S} 2b \left[ -\frac{\pi}{4} b \dot{W}_0 - \frac{\pi}{4} V W_1 - \frac{3\pi}{16} b \dot{W}_1 \right] \quad (11)$$

Drag acting along the resultant velocity :

$$D = \frac{1}{2}\rho \tilde{S} V^2 C_{D_o} \quad (12)$$

where $W_0$ and $W_1$ are defined as $W_0 = V(\theta + \frac{h}{V})$ and $W_1 = b\dot{\theta}$. The quantities $\dot{h}$, $\theta$ and V represent the heaving velocity at the elastic axis, the pitch angle and the oncoming velocity respectively.

ii) Modified ONERA Dynamic Stall Model (Ref. [36])

The modified dynamic stall model provides time variation of lift, moment and drag on an oscillating airfoil. The stall model assumes that the lift, moment and drag are acting at the quarter chord point. The unsteady lift acting normal to the resultant velocity is given as:

$$L = \frac{1}{2}\rho \tilde{S} \left[ sb \dot{W}_0 + \tilde{k} b \dot{W}_1 + V\Gamma_1 + V\Gamma_2 \right] \quad (13)$$

where $\Gamma_1$, $\Gamma_2$ are evaluated using the following equations.

$$\ddot{\Gamma}_1 + B_2\left(\frac{V}{b}\right)\dot{\Gamma}_1 + B_3\left(\frac{V}{b}\right)^2 \Gamma_1 = A_3\left(\frac{V}{b}\right)^2 \frac{\partial C_{z_L}}{\partial \theta} W_0$$

$$+ A_3 \sigma \left(\frac{V}{b}\right)^2 W_1 + A_2\left(\frac{V}{b}\right)\frac{\partial C_{z_L}}{\partial \theta}\dot{W}_0 + A_2 \sigma \left(\frac{V}{b}\right)\dot{W}_1$$

$$+ A_1 \frac{\partial C_{z_L}}{\partial \theta}\ddot{W}_0 + A_1 \sigma \ddot{W}_1$$

$$\ddot{\Gamma}_2 + a_l\left(\frac{V}{b}\right)\dot{\Gamma}_2 + r_l\left(\frac{V}{b}\right)^2 \Gamma_2 = -\left[ r_l\left(\frac{V}{b}\right)^2 V \Delta C_z|_{W_{0/V}} + E_l\left(\frac{V}{b}\right)\dot{W}_0 \right]$$

The unsteady moment on the airfoil is given as :

$$M = \frac{1}{2}\rho \tilde{S} 2b \left[ V^2 C_{m_L}|_{W_{0/V}} + (\bar{\sigma}_m + d_m) b \dot{W}_0 + \sigma_m V W_1 + s_m b \dot{W}_1 + V\Gamma_{m2} \right] \quad (14)$$

where $\Gamma_{m2}$ is evaluated using the following equation :

$$\ddot{\Gamma}_{m2} + a_m\left(\frac{V}{b}\right)\dot{\Gamma}_{m2} + r_m\left(\frac{V}{b}\right)^2 \Gamma_{m2} = -\left[ r_m\left(\frac{V}{b}\right)^2 V \Delta C_m|_{W_{0/V}} + E_m\left(\frac{V}{b}\right)\dot{W}_0 \right]$$

The unsteady drag acting along the resultant velocity is given as :

$$D = \frac{1}{2}\rho \tilde{S} \left[ V^2 C_{d_L}|_{W_{0/V}} + \sigma_d b \dot{W}_0 + V\Gamma_{d2} \right] \quad (15)$$

where $\Gamma_{d2}$ is evaluated using the following equation :

$$\ddot{\Gamma}_{d2} + a_d\left(\frac{V}{b}\right)\dot{\Gamma}_{d2} + r_d\left(\frac{V}{b}\right)^2 \Gamma_{d2} = -\left[ r_d\left(\frac{V}{b}\right)^2 V \Delta C_d|_{W_{0/V}} + E_d\left(\frac{V}{b}\right)\dot{W}_0 \right]$$

where $\Delta C_z|_{W_{0/V}}$, $\Delta C_m|_{W_{0/V}}$, and $\Delta C_d|_{W_{0/V}}$ are the difference between the linear static aerodynamic coefficient extrapolated to the stalled region to actual static aerodynamic coefficient of lift, moment and drag respectively, measured at an effective angle of attack $W_0/V$. The quantities, $C_{mL}|_{W_{0/V}}$, and $C_{dL}|_{W_{0/V}}$ are the static moment and drag coefficients in linear regime measured at an effective angle of attack, $W_0/V$.

Five different combinations of aerodynamic models have been proposed and the influence of each one of these models on the trim and response characteristics of helicopter rotor in forward flight is analysed systematically. The five aerodynamic models are:

- quasi-steady aerodynamic theory (Eqs.10-12) combined with uniform inflow model (Eq. 2) (QSUI),
- quasi-steady aerodynamic theory (Eqs.10-12) combined with Drees model (Eq.3) (QSDR),
- quasi-steady aerodynamic theory (Eqs.10-12) combined with dynamic wake model (Eq.4) (QSDW),

- modified ONERA stall model (Eqs.13-15) combined with Drees model (Eq.3) (DSDR); and
- modified ONERA stall model (Eqs.13-15) combined with dynamic wake model (Eq.4) (DSDW).

It may be noted that while describing the results only the abbreviations of the aerodynamic models are used for convenience.

Sectional aerodynamic loads are evaluated using either Eqs.10-12 or13-15. By summing up all the inertia and aerodynamic loads and integrating over the length of the blade, one can obtain the root loads. The root loads of all four rotor blades are added to obtain hub loads (H, Y, T, $M_x$, $M_y$ and $M_z$). Mean values of the hub loads are represented by $H_0$, $Y_0$, $T_0$, $M_{x0}$, $M_{y0}$ and $M_{z0}$.

**Tail Rotor**

The thrust generated by the tail rotor is derived using combined blade element and momentum theory. The tail rotor thrust acts normal to the tail rotor plane and in a direction providing compensation to the torque of the main rotor.

Tail rotor thrust is given by Ref. [37] :

$$T_T = C_{T_t}\left[\rho \pi R_t^2 (\Omega_t R_t)^2\right] \tag{16}$$

where the coefficient of tail rotor thrust $C_{T_t}$ is defined as :

$$C_{T_t} = \frac{\sigma_t a}{2}\left[\frac{\theta_{0T}}{3}\left(1+\frac{3}{2}\mu^2\right)-\frac{\lambda_t}{2}\right]$$

and tail rotor inflow is given by

$$\lambda_t = \frac{C_{T_t}}{2\sqrt{\mu^2+\lambda_t^2}}$$

**Horizontal Tail**

The horizontal tail is assumed to provide only aerodynamic lift. Lift is assumed as a point load acting at the quarter chord of the horizontal tail. The lift on horizontal tail is given as:

$$T_{HT} = \frac{1}{2}\rho\, s_h\, V_{HT}^2\, C_{l\theta_{ht}}\, \theta_{ht} \tag{17}$$

where $s_h$ is surface area and $V_{HT}$ is oncoming velocity, which is defined as :

$$V_{HT} = \begin{cases} \mu\,\Omega\,R & \mu < 0.05 \\ \left(\sqrt{\mu^2+(1.8\,\lambda)^2}\right)\Omega R & \mu \geq 0.05 \text{ (main rotor downwash effect is added)} \end{cases}$$

$\theta_{ht}$ is angle of attack and it is taken as -2 deg.

**Vertical Tail**

Vertical tail is assumed to provide a side force due to its lift. The load on vertical tail is obtained by using the static lift equation which is given below.

$$T_{VT} = \frac{1}{2}\rho\, s_v\, V_{VT}^2\, C_{l\theta_{vt}}\, \theta_{vt} \tag{18}$$

where $s_v$ is surface area and $\theta_{vt}$ is angle of attack and it is taken as 1.5 deg. The term $V_{VT}$ it is the oncoming velocity and is defined as:

$$V_{VT} = \mu\,\Omega\,R$$

**Fuselage Drag**

Fuselage drag force is proportional to the square of the velocity and the frontal area. Fuselage drag can be evaluated by using following expression.

$$D = \frac{1}{2}\rho\, V_F^2\, f\, C_d \tag{19}$$

where f is the equivalent frontal cross sectional area of the helicopter fuselage, $C_d$ is drag coefficient taken as 1.0 and $V_F$ is the oncoming velocity given as:

$$V_F = \mu\,\Omega\,R$$

**Equilibrium (or Trim) Equations**

Figure 1 shows the loads acting on the helicopter and the orientation of the helicopter in flight. Transferring all the forces and moments due to main rotor, tail rotor, horizontal tail, vertical tail and fuselage drag to centre of gravity (CG) of the helicopter and equating to the components of the gravitational load, the equilibrium equations are obtained. In this paper, only steady level flight condi-

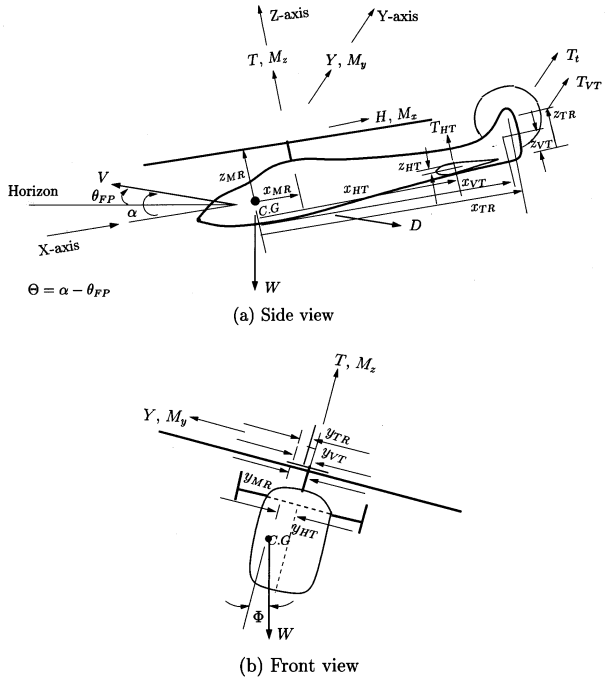


*Fig.1 Loads and Orientation of the Helicopter*

tions are considered; and hence inertia effects due to maneuver are not included. The force and moment equilibrium equations are given as:

$$H_0 + D \cos \alpha = W \sin \Theta \cos \Phi$$

$$Y_0 + T_T + T_{VT} = W \sin \Phi$$

$$T_0 + T_{HT} - D \sin \alpha = W \cos \Theta \cos \Phi$$

$$M_{x0} - Y_0 z_{MR} + T_0 y_{MR} - (T_T z_{TR} + T_{VT} z_{VT}) + T_{HT} y_{MR} = 0$$

$$M_{y0} - T_0 x_{MR} + H_0 z_{MR} - T_{HT} x_{HT} = 0$$

$$M_{z0} + Y_0 x_{MR} - H_0 y_{MR} + (T_T x_{TR} + T_{VT} x_{VT}) = 0 \qquad (20)$$

where $\Theta = \alpha - \theta_{FP}$. Trim variables ($\theta_0$, $\theta_{1c}$, $\theta_{1s}$, $\theta_{0T}$, $\Theta$ and $\Phi$) can be obtained by solving the above nonlinear algebraic equations (Eq. 20).

### Solution Procedure

The solution technique aims to obtain helicopter trim and blade response simultaneously by solving the three sets of equations in time domain, namely, (i) equations representing the elastic deformations of the rotor blade (Eq.1), (ii) equations representing the inflow through the rotor disc (Eq. 2, 3 or 4) and (iii) sectional aerodynamic loads representing lift, drag and moment acting on the rotor blade (Eqs. 10 - 12 or Eqs. 13 - 15). For the aerodynamic models QSUI, QSDR and QSDW, the sectional aerodynamic loads are represented by algebraic expressions given in Eqs. 10 - 12. Whereas, for the aerodynamic models DSDR and DSDW, the sectional aerodynamic loads have to be obtained by solving a set of differential equations in time domain given in Eqs. 13 - 15. Similarly, for the aerodynamic models involving time varying inflow, i.e., QSDW and DSDW, the inflow variables ($\alpha_1^0$, $\alpha_2^1$ and $\beta_2^1$) have to be obtained by solving the set of differential equations given in Eqs. 5 and 6. Of the five models used in this study, DSDW model is computationally more intensive than the other models. In this model, the time varying inflow, sectional aerodynamic loads and the blade response have to be solved by three sets of coupled ordinary differential equations, at every time step. A description on the number of variables for DSDW aerodynamic model is given in the following.

The aerodynamic loads acting on the blade are evaluated at 15 radial stations (starting from 0.25R to 0.95R with an increment of 0.05R) for each blade. Hence, there are in total 45 variables representing lift, drag and moment coefficients for one blade. It may be noted (from Eqs. 13 - 15) that there are four state variables for lift, two state variables each for drag and moment. Therefore, the total number of state variables representing the sectional aerodynamics for one blade is 120 (15 radial stations x 8 state variables per stations). The rotor blade structural model is represented by eight modes consisting of four flap modes, two lag modes, one torsion mode and one axial mode. Hence, the total number of state variables representing structural modes per blade is 16. The time varying inflow is given by three state variables. Therefore, for a four bladed rotor system, there are in total 547 state variables (480 aerodynamic state variables + 64 structural state variables + three state variables for dynamic wake effects). In the present study, a four bladed system with proper spacing in the azimuth angle is considered for the analysis. By solving the response of all the blades simultaneously, one can identify the difference in the response of the blades as they go around the azimuth. Since, the response and loads of all the blades are solved at every instant of time, the time varying hub loads and the time varying inflow (dynamic wake effects) can be captured.

**Flow Chart and Algorithm**

A propulsive trim procedure has been adopted to obtain the main rotor control angles, tail rotor collective angle, fuselage roll and pitch attitudes. A fourth order Runge-Kutta integration scheme with a time step $\Delta t$ = 0.0025 sec., has been used for solving the differential equations. Flow chart for the calculation of helicopter trim and rotor response is shown in the Fig.2. The steps involved in the evaluation of trim and response using DSDW model (which is computationally intensive as compared to other four models) are described below. These steps get simplified appropriately while using the other four models, namely, QSUI, QSDR, QSDW and DSDR.

- For a given data including flight condition, evaluate mean rotor inflow based on all-up weight.
- Assume initial values for trim variables ($\theta_0$, $\theta_{1c}$, $\theta_{1s}$, $\theta_{0T}$, $\Theta$ and $\Phi$) and initial conditions for blade response.
- Knowing rotor inflow and blade response and obtain the sectional aerodynamic loads for all the blades, by solving the dynamic stall equations.

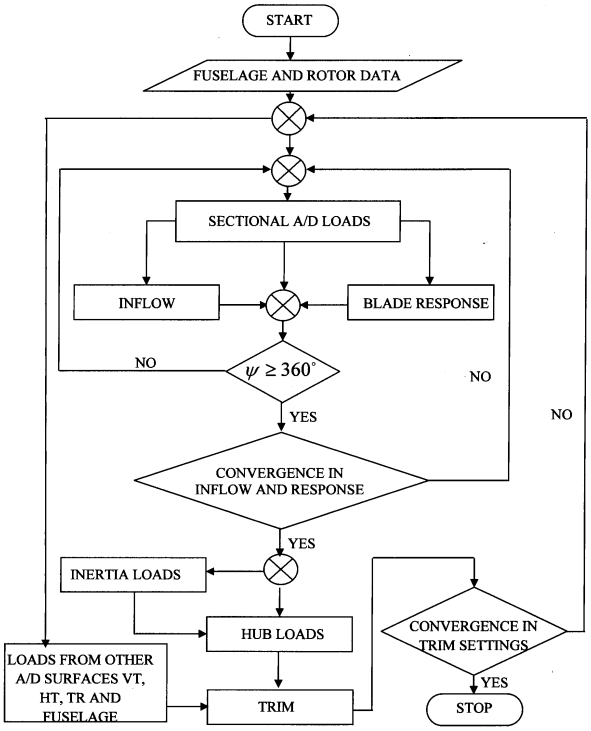


VT – Vertical Tail; HT – Horizontal Tail; TR – Tail Rotor

*Fig.2 Flow Chart for Calculation of Helicopter Trim and Rotor Response*

- Then using the sectional blade loads, the response of individual blades and rotor inflow variables are obtained simultaneously for the next time step, using blade equations and dynamic wake equations respectively.
- Next, by using the blade response and inflow, go to step 3. This iteration is performed for about 40-50 rotor revolutions till convergence in the blade response and inflow variables are obtained.
- Using the converged blade response, the blade root loads and hub loads are obtained.
- Then transfer the mean values of rotor hub loads, loads from horizontal tail, vertical tail, tail rotor and fuselage to the CG to satisfy the trim equations (Eq. 20).
- Evaluate improved trim variables using Newton-Raphson technique.
- Go to step 2. The iterations are continued till convergence in trim variables achieved. The convergence criterion is based on satisfying the condition that the difference in each trim setting between two successive iterations must be less than 0.002%.

**Results and Discussion**

Using the solution technique described in the previous section, helicopter trim and aeroelastic response of the rotor blades are analysed for different cases to bring out: (i) the effect of aerodynamic modeling ,(ii) the influence of forward speed and (iii) the influence of structural couplings due to blade pretwist on loads and response. Three sets of results are presented in the following. First set of results pertains to trim, second set of results corresponds to loads and response for different forward speed conditions and last set of results is related to twisted blade configuration. Even though the response of all the blades in the rotor system is evaluated independently, for conciseness, in the description of the results only the response and loads of blade-1 (reference blade) are presented. The geometric description of the helicopter is shown in Fig.1. The main rotor blade is modeled as a soft-in plane hingeless rotor blade with eight elastic modes representing four flap, two lag, one torsion and one axial modes. The rotor system consists of four blades. The data used in the present study are given in Tables-1 and 2.

**Trim**

Using the five different aerodynamic models (QSUI, QSDR, QSDW, DSDR and DSDW), helicopter trim and

| **Table-1 : Helicopter Data** | |
|---|---|
| Variable | **Quantity** |
| Number of blades, Nb | 4 |
| Air density at sea level, $\rho$ (kg/m$^3$) | 1.224 |
| Weight of the helicopter, W (N) | 45000 |
| Mass of the helicopter, (kg) | 4592 |
| Mass of main rotor blade, $M_b$ (kg) | 55.4 |
| Radius of the main rotor blade, R (m) | 6.6 |
| Radius of the tail blade, $R_t$ (m) | 1.3 |
| Chord of the main rotor blade, C (m) | 0.5 |
| Chord of the tail rotor blade, $C_t$ (m) | 0.19 |
| Main rotor rotating sped, $\Omega$ (rpm) | 300 |
| Tail rotor rotating speed, $\Omega_t$ (rpm) | 1500 |
| Fuselage frontal area, f (m$^2$) | 1.8 |
| Horizontal tail area, $S_h$, (m$^2$) | 2.24 |
| Vertical tail area, $S_v$, (m$^2$) | 2.126 |
| Blade loading, $C_T/\sigma$ | 0.0648 |
| Blade frequency data (Untwisted) : | |
| Flap mode | 1.089, 2.896, 5.145, 7.688 |
| Lag mode | 0.701, 5.308 |
| Torsional mode | 4.509 |
| Axial mode | 9.155 |

| **Table-2 : Geometrical Data of the Helicopter** | |
|---|---|
| Variable | **Quantity (m)** |
| $X_{MR}$ | 0.0 |
| $X_{HT}$ | 7.5 |
| $X_{VT}$ | 7.5 |
| $X_{TR}$ | 7.5 |
| $Y_{MR}$ | 0.0 |
| $Y_{HT}$ | 0.0 |
| $Y_{VT}$ | 0.0 |
| $Y_{TR}$ | 0.0 |
| $Z_{MR}$ | 2.0 |
| $Z_{HT}$ | 0.5 |
| $Z_{VT}$ | 1.75 |
| $Z_{TR}$ | 2.0 |

blade response are evaluated for different forward speed conditions. The variation of control angles ($\theta_0$, $\theta_{1c}$, $\theta_{1s}$ and $\theta_{0T}$ ) and the fuselage attitude in pitch ($\Theta$) and roll ($\Phi$) with forward speed are shown in Fig.3. From Fig.3a, it can be seen that the magnitude of the collective pitch angle ($\theta_0$) is affected by the aerodynamic models used in the analysis. However, at high forward speeds ($\mu > 0.25$), the aerodynamic models do not significantly influence the collective pitch angle. It is observed that the models with dynamic wake (QSDW and DSDW) require high collective pitch setting at low forward speeds than the other aerodynamic models. For hover, the variation in the collective pitch angle for all these models is of the order 0.75 deg. A similar observation can be made for the tail rotor collective pitch ($\theta_{0T}$) as shown in Fig.3d.

The variation of the lateral cyclic control angle ($\theta_{1c}$) with forward speed is shown in Fig.3b. From the figure, it can be seen that inclusion of Drees model with quasi-steady aerodynamics (QSDR) increases the control angle

in the transition zone (i.e., in the range $\mu$ = 0.05 to 0.075). The increase is more pronounced if dynamic wake model is used (QSDW) instead of Drees model. In this transition zone, dynamic stall model has very little effect but as $\mu$ increases dynamic stall model shows more reduction in control angle as compared to quasi-steady aerodynamics. This type of sharp rise and fall in the variation of $\theta_{1c}$ obtained with DSDW model qualitatively resembles the flight data presented in Ref. [38]. Dynamic stall models require more longitudinal cyclic control angle ($\theta_{1s}$) at high forward speeds as can be seen in Fig.3c. The equilibrium roll angle of the helicopter (as observed in Fig.3e) is larger for QSUI model as compared to other four aerodynamic models. The equilibrium roll angle is the least for the two dynamic wake models DSDW and QSDW; and the roll angles are found to be almost the same for these two models. It is interesting to note from Fig.3f that the pitch attitude of the helicopter shows a monotonic increase with forward speed; but at high forward speeds there is a slight reduction in the pitch angle for the two dynamic stall models DSDR and DSDW.

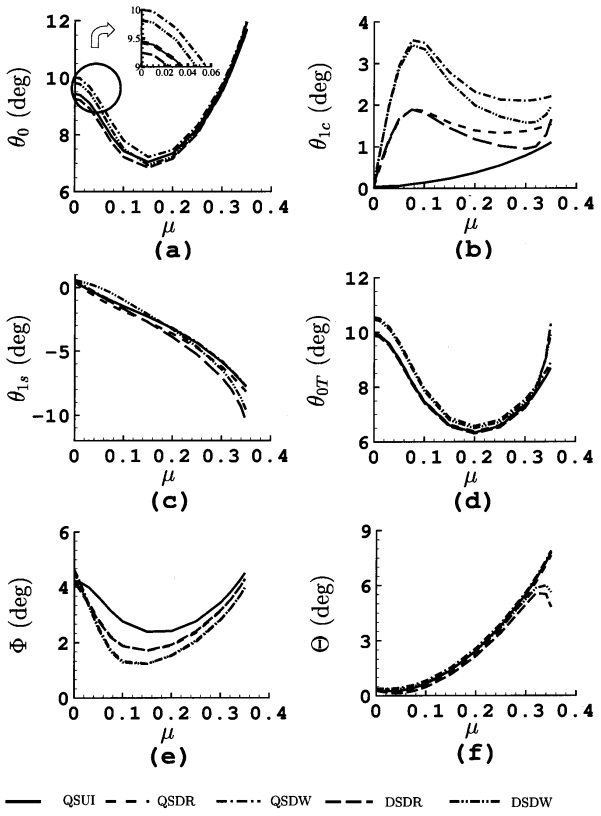


*Fig.3 Variation of Trim Angles with Forward Speed* $\mu$

**Effect of Forward Speed**

Using DSDW aerodynamic model, sectional aerodynamic loads at various radial stations, blade root loads and hub loads are evaluated for different forward speed conditions. Contour plots showing the effective angle of attack on rotor disk are shown in Figs.4 and 5 for low and high forward speeds, respectively. At very low forward speed, $\mu$ = 0.01 (Fig.4), the effective angle of attack is found to vary between -3 deg. to 6 deg., whereas at high forward speed (Fig.5) the effective angle of attack is varies from 17 deg. to -130 deg. (in reverse flow region).

The variation of sectional lift, drag and moment versus azimuth angle are shown in Figs.6 - 8. From Fig.6, it can be seen that the magnitudes of the sectional lift is affected by the forward speed. At low forward speeds ($0 < \mu < 0.1$), sectional lift exhibits one/rev variation with small amplitude. Whereas, high forward speeds introduce large variation in the sectional lift with additional harmonics. One interesting observation from Figs.6a - 6e is that the occurrence of minimum value of the sectional lift force in the forward speed range $0.2 < \mu < 0.3$, shifts from retreating side to advancing side as the radial station moves from in-board towards the tip. Whereas for $\mu$ = 0.35, the minimum value of the sectional lift is almost the same in both advancing and retreating sides. The reason for this phenomenon can be attributed to stall in the retreating side.

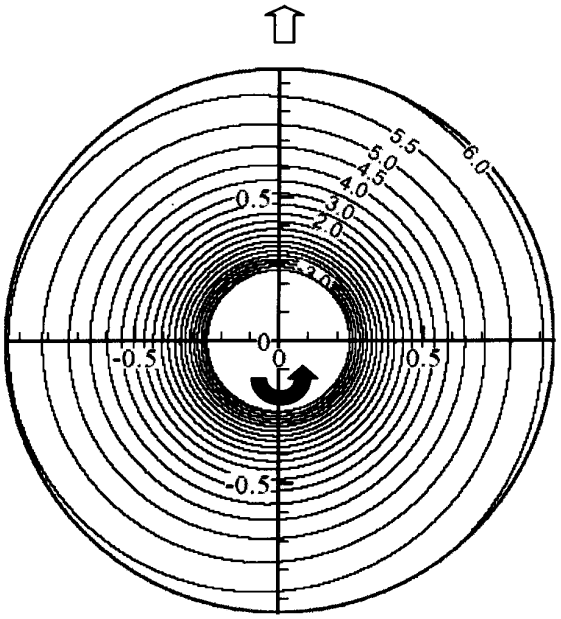


*Fig.4 Effective Angle of Attack on Rotor Disk at m = 0.01 (Angles are deg)*

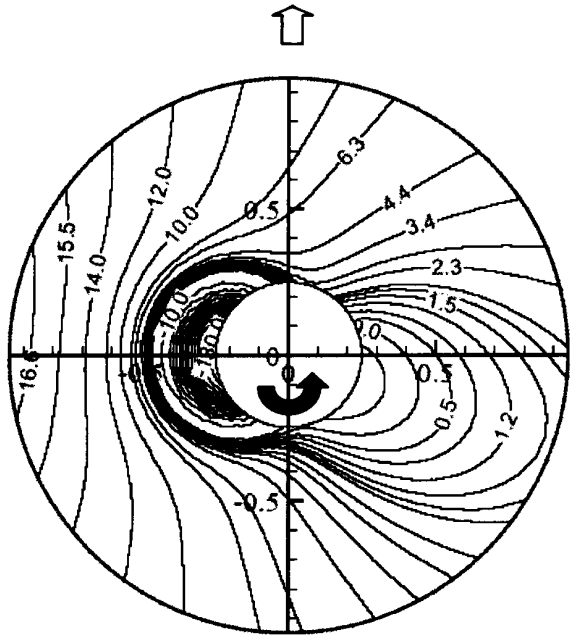


*Fig.5 Effective Angle of Attack on Rotor Disk at m = 0.35 (Angles are deg)*

Figures 7 and 8 show the variation of sectional drag and moment at different radial stations, respectively. With increase in forward speed, sectional drag shows large variation in all radial stations. For the high forward speed $\mu = 0.35$, the sectional drag (Fig.7) shows a large increase near the tip region (85%R and 95%R) in the retreating side ($230 < \psi < 360$ deg) due to dynamic stall effects. A similar observation is also seen in the case of sectional torsional moment as shown in Fig.8.

For the reference blade (blade-1), the variation of root forces and root moments with azimuth angle are shown in Figs. 9 and 10, respectively. As the forward speed increases, the amplitude of root forces and moments increase substantially. At low forward speeds ($0 < \mu < 0.1$), the maximum value of root force $Fx_{1k}$ occurs around 90 deg. azimuth, and the maximum value of $Fy_{1k}$ occurs around 180 deg. azimuth. Whereas, at high forward speeds the peak value of root force $Fx_{1k}$ shifts to 10 deg. azimuth and the corresponding peak of $Fy_{1k}$ moves to 90 deg. azimuth (Figs.9a and 9b). From Fig.9c, it is clear that as the forward

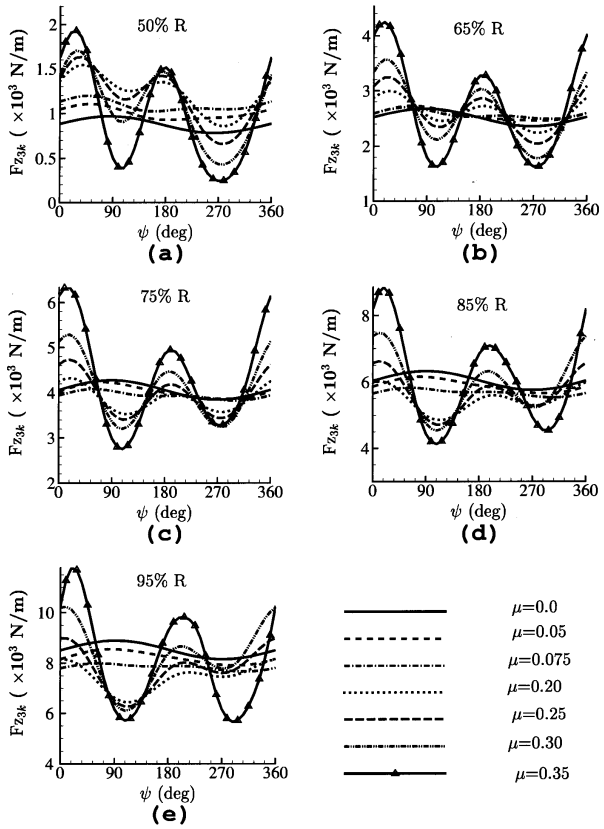


*Fig.6 Variation of Sectional Aerodynamic Lift for Different Forward Speeds*

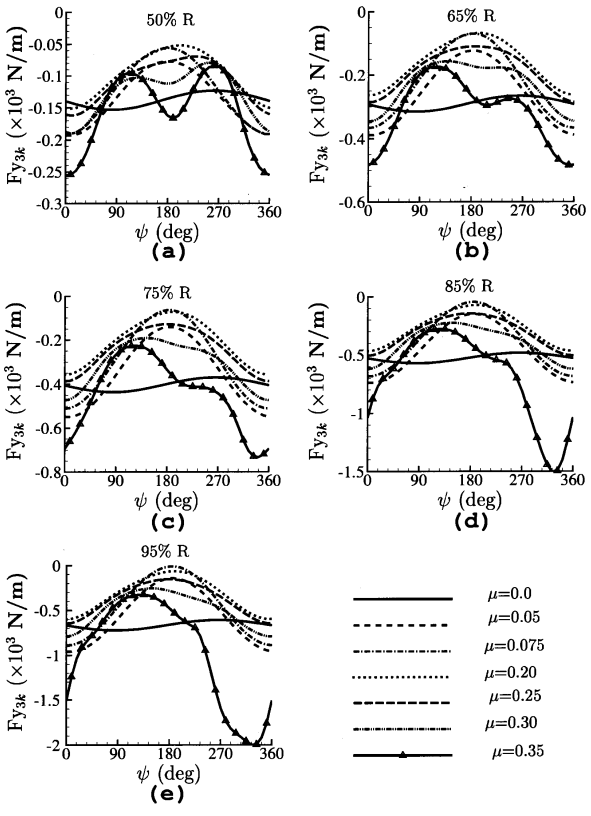


*Fig.7 Variation of Sectional Aerodynamic Drag for Different Forward Speeds*

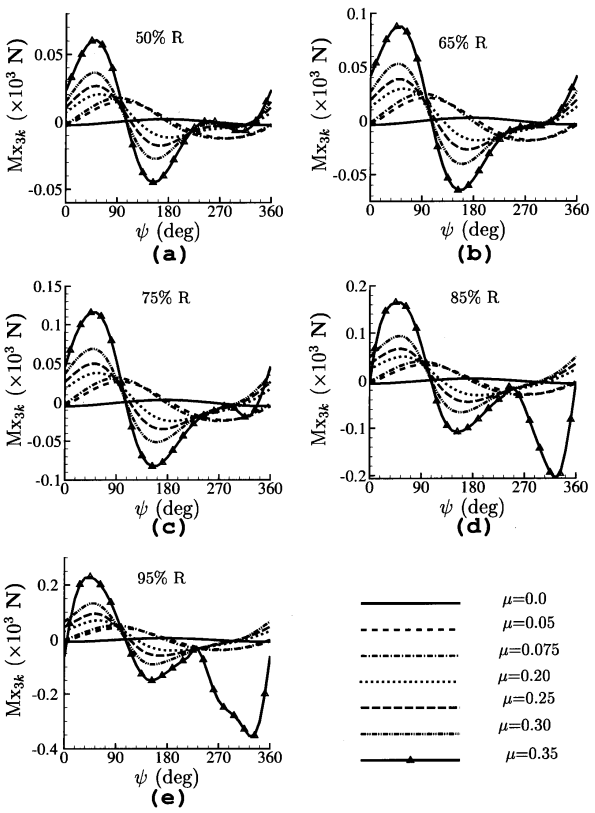


*Fig.8 Variation of Sectional Aerodynamic Moment for Different Forward Speeds*

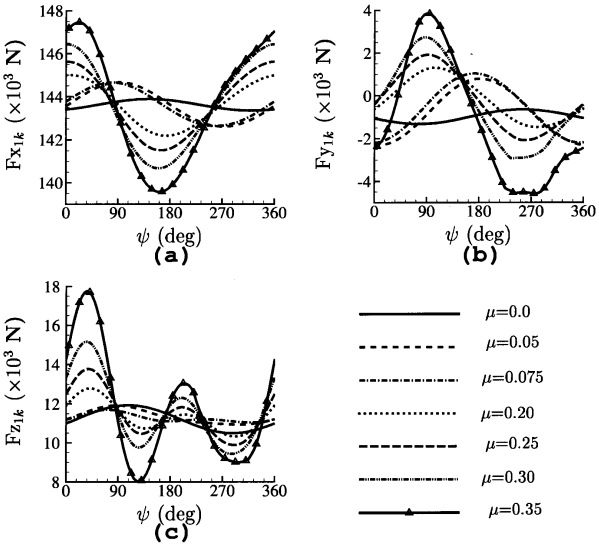


*Fig.9 Blade Root Forces for Different Forward Speeds*

speed increases, the peak to peak variation of root shear force $Fz_{1k}$ increases substantially. Root torsional moment $Mx_{1k}$ (Fig. 10a) shows a very small variation in hover and a substantial increase at advance ratio $\mu = 0.35$. Whereas in the speed range $\mu = 0.05$ to 0.3 the torsional moment shows a gradual increase with forward speed. The response of root moment in flap $My_{1k}$ (Fig.10b) shows a trend which is opposite to that of root shear $Fz_{1k}$ (Fig.9c). The reason for the opposite trend is due to the sign convention used for flap moment (flap up provides negative moment). The response of root moment in lead-lag $Mz_{1k}$ (Fig.10c) shows a trend which is similar to that of root shear $Fy_{1k}$ (Fig.9b).

The variation of hub forces and moments over one revolution of the rotor is shown in Figs.11 and 12, respectively. The variations of loads show dominant 4/rev oscillatory component with increase in forward speed. As the forward speed increases, the mean value of the hub forces and moments changes significantly.

Figure 13 shows the tip response of the blade in flap, lag and torsional modes. In all the modes, the tip response shows a monotonic increase with increase in forward speed. For the forward speed $\mu = 0.35$, additional harmonics are introduced in torsional response due to dynamic stall effects.

**Effect of Structural Coupling Due to Pretwist**

The purpose of this study is to analyse the effects of structural coupling due to blade pretwist on loads, and

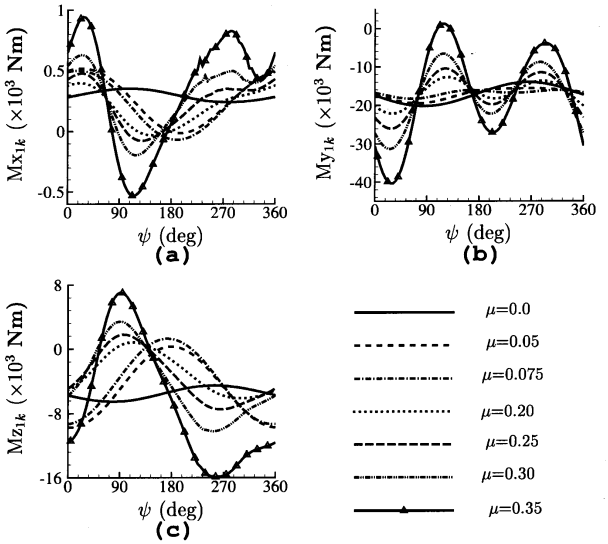


*Fig.10 Blade Root Moments for Different Forward Speeds*

aeroelastic response of the rotor blade. Four different values of pretwist, namely -4 deg, -8 deg, -12 deg, and -16 deg are considered. In all these configurations, the tip pitch angle is set at 4 deg. For example, for a blade configuration with -8 deg pretwist, if the control pitch input is zero, then the root pitch angle of the blade is 12 deg and the tip pitch angle is 4 deg. In the following, comparison of sectional aerodynamic loads and blade tip response for straight and twisted blade configurations is presented.

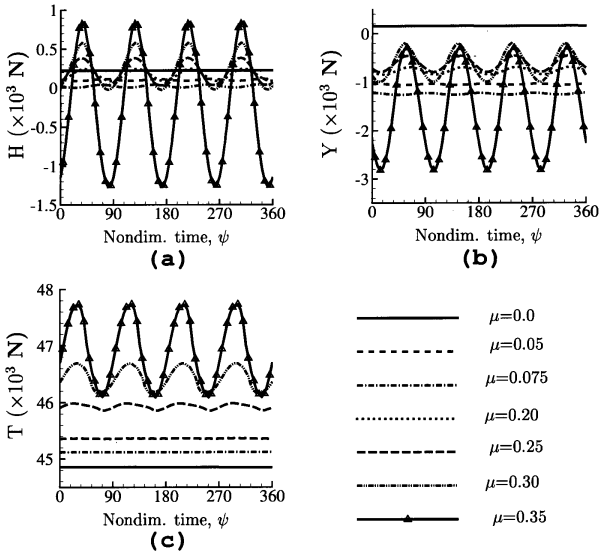


*Fig.11 Hub Forces for Different Forward Speeds*

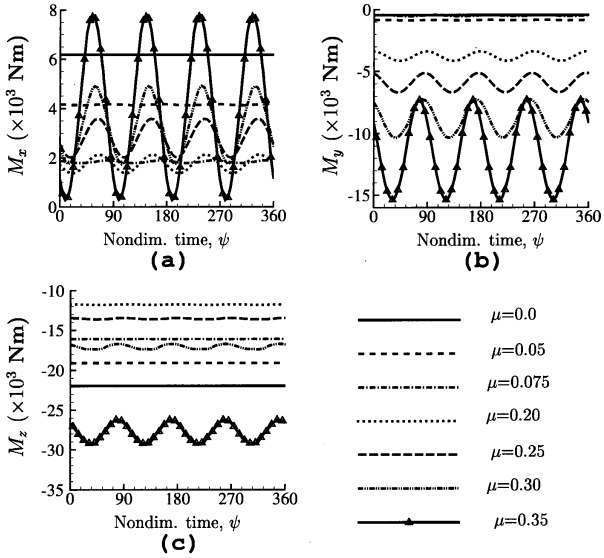


*Fig.12 Hub Moments for Different Forward Speeds*

Sectional aerodynamic lift, drag and moment at various radial stations (50%R, 65%R, 75%R, 85%R and 95%R) are shown respectively in Figs.14-16, for one blade as it goes around the azimuth, for an advance ratio $\mu$ = 0.35. From the Fig.14, it can be seen that for the case of straight blade configuration, the minimum value of the sectional lift force is almost the same in both advancing and retreating sides at all the radial stations. Whereas, for the case of twisted blade configuration, the occurrence of minimum value of the sectional lift force shifts from retreating side to advancing side as the radial station moves towards the tip. From Fig.15, it is observed that at the out-board stations (85%R and 95%R), the variation in sectional drag force is considerably small for the twisted blade configuration as compared to straight blade configuration. These results show that the effect of dynamic stall is reduced in the retreating side due to blade pretwist. From Fig.16, it is observed that the sectional moment shows identical variation at in-board sections (50%R and 65%R) for both twisted and straight blade configurations. At the out-board stations (85%R and 95%R), the sectional moment undergoes a large variation in the retreating side for

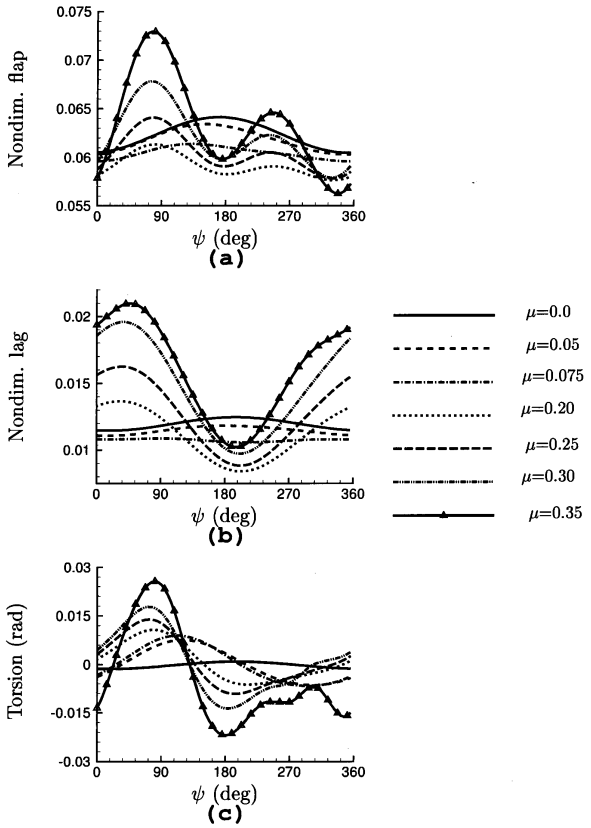


*Fig.13 Tip Response for Different Forward Speeds*

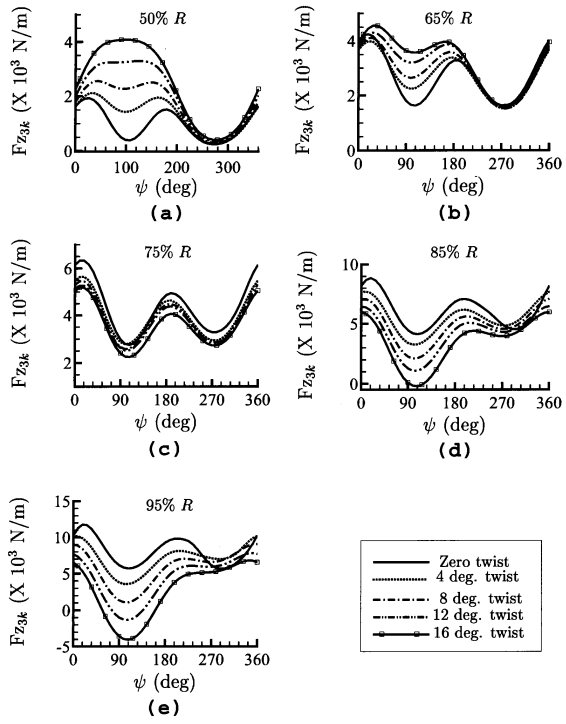


*Fig.14 Sectional Lift for Various Twisted Blade Configurations for μ = 0.35*

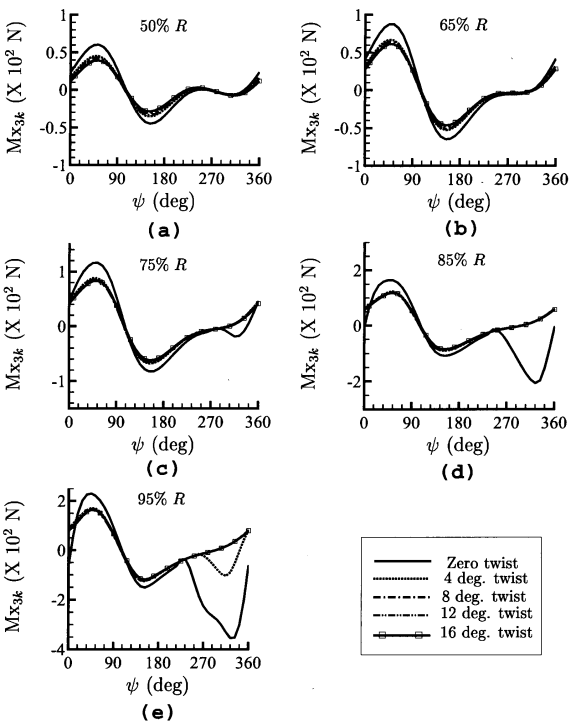


*Fig.16 Sectional Moment for Various Twisted Blade Configurations for μ = 0.35*

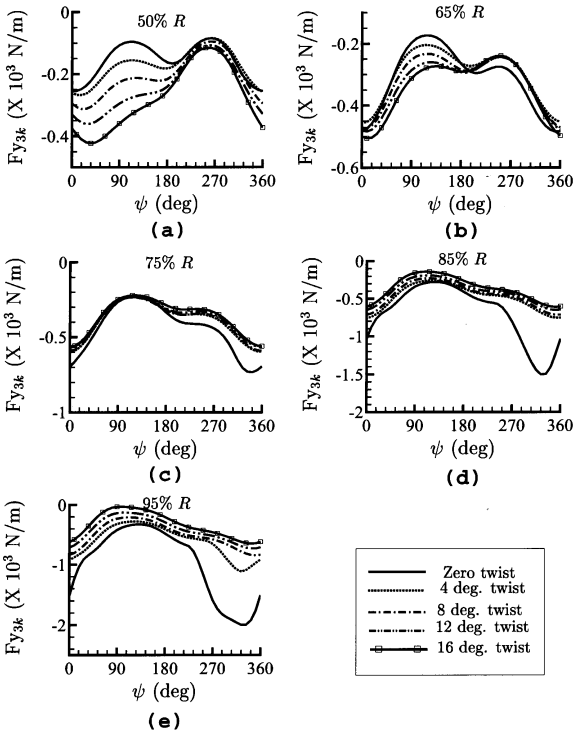


*Fig.15 Sectional Drag for Various Twisted Blade Configurations for μ = 0.35*

the straight blade as compared to the twisted blade configuration.

The tip response of a single blade in flap, lap and torsional modes is shown in Fig.17. The magnitude of the variation of the tip response is relatively small for the case of twisted blade configuration as compared to the straight blade configuration. Fig.17c shows that the torsional response has more harmonics as compared to flap and lag response. Variation in pretwist seems to have more influence on the mean values of flap and lag deformations, as compared to the mean value of torsional deformation. Mean value of flap and lag deformations decrease with increase in pretwist upto a value of -12 deg and then it increases for -16 deg pretwist.

The variation of root loads for a single blade as it goes around the azimuth is shown in Fig.18. From the figure, it can be seen that there is a reduction in the magnitudes of the root loads for the case of twisted blade configuration as compared to the straight blade configuration. Various harmonics of the blade root loads are shown in Fig.19. This figure shows several interesting features. Inclusion of pretwist reduces all the harmonic contents for the root loads $F_{x1k}$, $F_{y1k}$ and $M_{z1k}$ (i.e., Figs.19a,19b and 19f). For

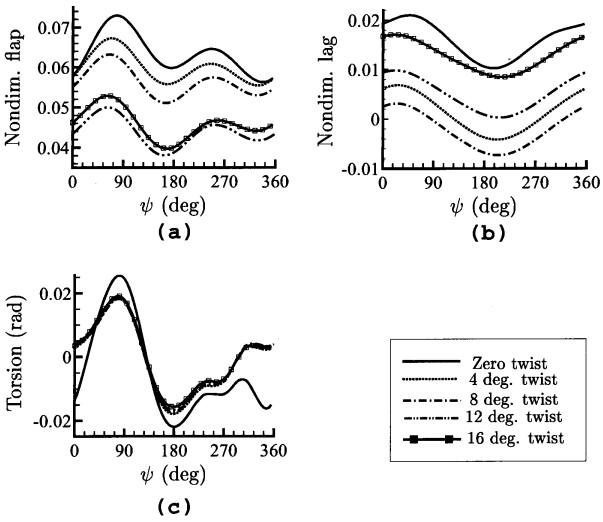


*Fig.17 Tip Deformations of the Rotor Blade for Various Twisted Blade Configurations for μ = 0.35*

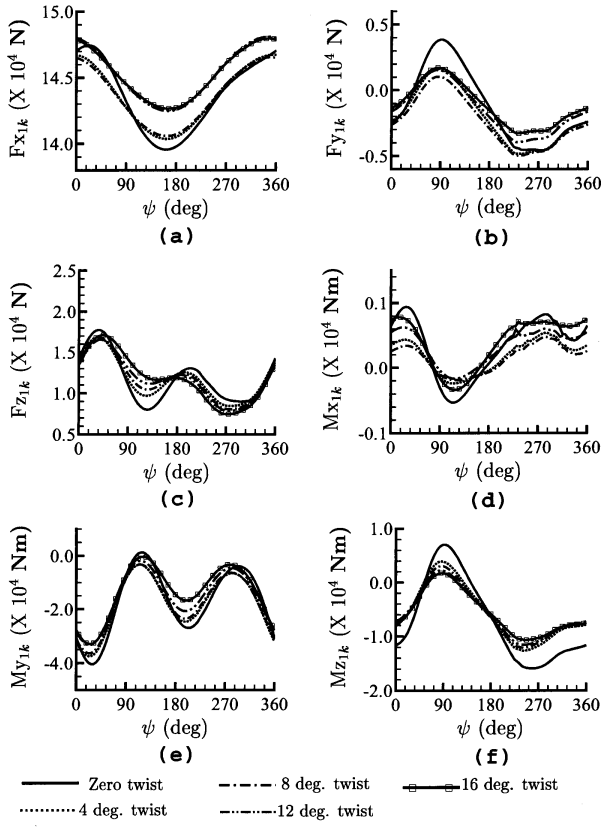


*Fig.18 Root Loads for Various Twisted Blade Configurations for μ = 0.35*

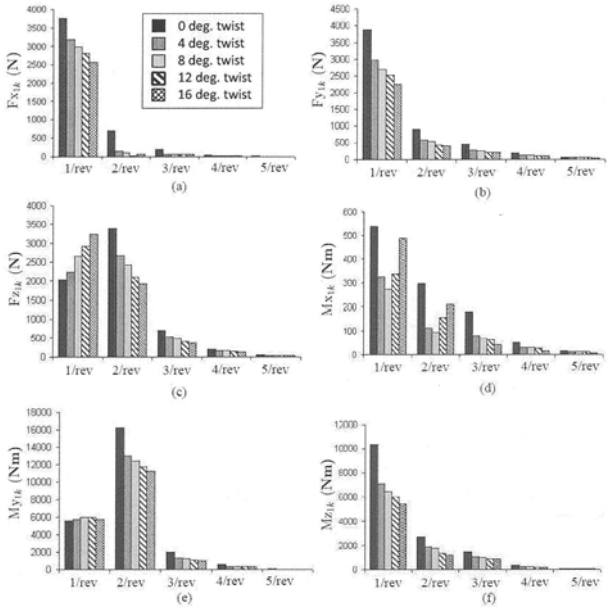


*Fig.19 Harmonics of Root Loads for Various Twisted Blade Configurations for μ = 0.35*

the case of vertical root shear $F_{z1k}$ (Fig.19c), 1/rev component shows an increase with increase in pretwist and all the other components show a reduction with increase in pretwist. For the case of root torsional moment $M_{x1k}$ (Fig.19d), -8 deg pretwist provides a minimum value of 1/rev and 2/rev components, whereas inclusion of twist shows a monotonic reduction in higher harmonic components. In the case of root flap moment $M_{y1k}$ (Fig.19e), there is no appreciable change in 1/rev component, whereas there is a reduction in other harmonic contents with inclusion of pretwist.

## Concluding Remarks

A computational aeroelastic model has been developed, wherein the equations representing the blade dynamics, rotor inflow and sectional aerodynamics including stall are solved in a sequential manner. A four bladed system with proper spacing in the azimuth angle has been considered for the analysis. By solving simultaneously the response of all the blades, one can identify the difference in the response of the blades as they go around the azimuth. Since the response and loads of all the blades are solved at every instant of time, the time varying hub loads and time varying inflow (dynamic wake effects) can be captured. A systematic study is undertaken to analyse the influence of five different aerodynamic models, representing rotor inflow and sectional aerodynamic loads, on the helicopter trim and aeroelastic response of the rotor

blades. The effect of pretwist on the helicopter loads and aeroelastic response of the rotor blades is also studied.

The important observations of this study can be summarised as:

- The lateral cyclic pitch ($\theta_{1c}$) setting required for trim is significantly affected by rotor inflow at low forward speeds ($0 < \mu < 0.1$), and by dynamic stall effects at forward speeds ($\mu > 0.15$). It is also found that the aerodynamic model, incorporating dynamic wake and dynamic stall effects, predicts the trim parameter ($\theta_{1c}$) whose variation with forward speed resembles closely to those obtained in flight test.
- At low forward speeds ($0 < \mu < 0.1$), the sectional lift at various cross-sections of the blade, exhibits one/rev variation with small amplitude. Whereas, high forward speeds introduce large variation in the sectional lift with additional harmonics.
- At high forward speeds, dynamic stall effects significantly increase the torsional response of the rotor blade.
- The structural coupling due to blade pretwist is observed to significantly alter the time variation of the sectional loads as compared to the loads obtained for a straight untwisted blade. This result indicates that aeroelastic coupling due to blade pretwist has a significant influence on the rotor loads.

## Acknowledgment

The authors acknowledge the financial support provided by the Department of Science and Technology, India.

## References

1. Friedmann, P. P., "Renaissance of Aeroelasticity and Its Future", Journal of Aircraft, Vol. 36, No. 1, 1999, pp. 105-121.

2. Friedmann, P. P and Hodges, D. H., "Rotary Wing Aeroelasticity - A Historical Perspective", Journal of Aircraft, Vol. 40, No. 6, 2003, pp. 1019-1046.

3. Friedmann, P. P., "Rotary Wing Aeroelasticity: Current Status and Future Trends", AIAA Journal, Vol. 42, No. 10, 2004, pp. 1953-1972.

4. Hodges, D. H., "Review of Composite Rotor Blade Modeling", AIAA Journal, Vol. 28, No. 3, 1990, pp. 561-564.

5. Johnson, W., "Rotorcraft Dynamics Models for a Comprehensive Analysis", Proceedings of the 54th Annual Forum of the American Helicopter Society, Washington, D.C., 1998.

6. Hodges, D. H., Saberi, H and Ormiston, R. A., "Development of Nonlinear Beam Elements for Rotorcraft Comprehensive Analyses", Journal of the American Helicopter Society, Vol. 52, No. 1, 2007, pp. 36-48.

7. Gaonkar, G. H and Peters, D. A., "Flap-Lag Stability with Dynamic Inflow by the Method of Multiblade Coordinates", Presented at the 20th AIAA /ASME /ASCE / AHS Structures, Structural Dynamics, and Materials Conference, St. Louis, Missouri, April 4-6, 1979.

8. Gaonkar, G. H and Peters, D. A., "Use of Multiblade Coordinates for Helicopter Flap-Lag Stability with Dynamic Inflow", Journal of Aircraft, Vol. 17, No.2, 1980, pp.112-118.

9. Gaonkar, G. H and Peters, D. A., "Effectiveness of Current Dynamic-Inflow Models in Hover and Forward Flight", Journal of the American Helicopter Society, Vol. 31, No. 2, 1986, pp. 47-57.

10. Peters, D. A and HaQuang, N., "Dynamic Inflow for Practical Application", Journal of the American Helicopter Society, Vol. 33, No. 4, 1988, pp. 64-68.

11. Su, A., Yoo, K. M and Peters, D. A., "Extension and Validation of an Unsteady Wake Model for Rotors", Journal of Aircraft, Vol. 29, No. 3, 1992, pp. 374-383.

12. Peters, D. A and Su, A., "Effect of an Unsteady Three-Dimensional Wake on Elastic Blade-Flapping Eigenvalues in Hover", Journal of the American Helicopter Society, Vol. 38, No. 1, 1993, pp. 45-54.

13. Manjunath, A. R., Nagabhushanam, J., Gaonkar, G. H., Peters, D. A and Su, A., "Flap-Lag Damping in Hover and Forward Flight With a Three-Dimensional Wake", Journal of the American Helicopter Society, Vol. 38, No. 4, 1993, pp. 37-49.

14. Manjunath, A. R., Chunduru, S. J., Nagabhushanam, J and Gaonkar, G. H., "Flap-Lag-Torsion Stability in Hover and Forward Flight With a Three-Dimensional Wake", AIAA Journal, Vol. 34, No. 1, 1996, pp. 18-28.

15. Nagabushanam, J and Gaonkar, G. H., "Hingeless Rotor Aeromechanical Stability in Axial and Forward Flight With Wake Dynamics", Journal of the American Helicopter Society, Vol. 44, No. 3, 1999, pp. 222-233.

16. Tran, C. T and Falchero, D., "Application of the ONERA Dynamic Stall Model to a Helicopter Blade in Forward Flight", 7th European Rotorcraft and Power Lift Aircraft Forum, Garmisch-Partenkirchen, F.R.G., Sept. 8-11, 1981.

17. Rogers, J. P., "Application of an Analytic Stall Model to Time-History and Eigenvalue Analysis of Rotor Blades", 8th European Rotorcraft Forum, Aix-en-Provence, France, Sept. 1982.

18. Bergh, H and Van der Wekken, J. P., "Comparison Between Measured and Calculated Stall-Flutter Behaviour of a One-Bladed Model Rotor", Vertica, Vol. 11, No. 3, 1987, pp. 447-456.

19. Dunn, P and Dugundji, J., "Nonlinear Stall Flutter and Divergence Analysis of Cantilevered Graphite/Epoxy Wings", AIAA Journal, Vol. 30, No. 1, 1992, pp. 153-162.

20. Tang, D and Dowell, E. H., "Comparison of Theory and Experiment For Non-linear Flutter and Stall Response of a Helicopter Blade", Journal of Sound and Vibration, Vol. 165, No. 2, 1993, pp. 251-276.

21. Barwey, D., Gaonkar, G. H and Ormiston, R. A., "Investigation of Dynamic Stall Effects on Isolated Rotor Flap-Lag Stability with Experimental Correlation", Journal of the American Helicopter Society, Vol. 36 No. 4, 1991, pp. 12-24.

22. Barwey, D and Gaonkar, G. H., "Investigation of Dynamic Stall Effects on Isolated Rotor Flap-Lag Stability with Experimental Correlation", AIAA Journal, Vol. 32, No. 4, 1994, pp. 811-819.

23. Tang, D and Dowell, E. H., "Damping Prediction for a Stalled Rotor in Flap-Lag with Experimental Correlation", Journal of the American Helicopter Society, Vol. 40 No. 4, 1995, pp. 79-89.

24. Peters, D. A., Barwey, D and Su, A., "An Integrated Airloads - Inflow Model for Use in Rotor Aeroelasticity and Control Analysis", Mathematical and Computer Modelling, Vol.19, No. 3/4, 1994, pp.109-123.

25. Chunduru, S. J., Subramanian, S and Gaonkar, G. H., "Dynamic Stall and Wake Effects on Trim and Stability of Hingeless Rotors with Experimental Correlation", Journal of the American Helicopter Society, Vol. 42, No. 4, 1997, pp. 370-382.

26. Subramanian, S., Ma, G., Gaonkar, G. H and Maier, T. M., "Correlation of Several Aerodynamic Models and Measurements of Hingeless - Rotor Trim and Stability", Journal of the American Helicopter Society, Vol. 45, No. 2, 2000, pp. 312-318.

27. Postsdam, M., Yeo, H and Johnson, W., "Rotor Airloads Prediction Using Loose Aerodynamic/ Structural Coupling", Journal of Aircraft, Vol. 43, No. 3, 2006, pp. 732-742.

28. Datta, A and Chopra, I., "Prediction of UH-60A Dynamic Stall Loads in High Altitute Level Flight Using CFD/CSD Coupling", Proceedings of the 61st Annual Forum of the American Helicopter Society, Washington D.C., 2005.

29. Bhagwat, M. J., Ormiston, R. A., Saberi, H. A and Xin, H., "Application of CFD/CSD Coupling for Analysis of Rotorcraft Airloads and Blade Loads in Maneuvering Flight", Proceedings of the 63rd Annual Forum of the American Helicopter Society, Washington D.C., 2007.

30. Lytwyn, R. T., "An Analysis of the Divergent Vertical Helicopter Oscillations Resulting from the Physical Presence of the Pilot in the Collective Control Loop", Proceedings of the 22nd Annual Forum of the American Helicopter Society, Washington, D.C., 1966.

31. Bousman, W. G., "Putting the Aero Back Into Aeroelasticity", Proceedings of the 8th Annual Workshop on Aeroelasticity of Rotorcraft Systems, University Park, PA, USA, 1999.

32. Prasad, C. G. N., Dwivedi, V and Dutta, R., "Vibration Monitoring in Helicopter Structure Using Rotor Noise: Flight Test Results and Discussions", Proceedings of the 15th National Seminar on Aerospace Structure, Shree Maruthi Publishers, Coimbatore, India, 2007, pp. 161-165.

33. Yuan, K. A and Friedmann, P. P., "Aeroelasticity and Structural Optimization of Composite Helicopter Rotor Blades with Swept Tips", NASA Report 4665, May 1995.

34. He, Cheng Jian., "Development and Application of a Generalized Dynamic Wake Theory for Lifting Rotors", Ph.D. Thesis, Georgia Institute of Technology, July 1989.

35. Greenberg, M. J., "Airfoil in Sinusoidal Motion in a Pulsating Stream", NASA Technical Report 1326, 1947.

36. Laxman, V and Venkatesan, C., "Chaotic Response of an Airfoil due to Aeroelastic Coupling and Dynamic Stall", AIAA Journal, Vol. 45, No. 1, 2007, pp. 271-280.

37. Venkatesan, C., "Lecture Notes on Helicopter Technology", Department of Aerospace Engineering, Indian Institute of Technology Kanpur, India.

38. Padfield, G. D., "Helicopter Flight Dynamics", Blackwell Science Ltd, 1996.